Shaping post-orogenic landscapes by climate and chemical weathering

Oliver A. Chadwick[1]*, Josh J. Roering[2], Arjun M. Heimsath[3], Shaun R. Levick[4], Gregory P. Asner[5], and Lesego Khomo[6]
[1]Department of Geography, University of California–Santa Barbara, Santa Barbara, California 93106, USA
[2]Department of Geological Sciences, University of Oregon, Eugene, Oregon 97403, USA
[3]School of Earth and Space Exploration, Arizona State University, Tempe, Arizona 85287, USA
[4]Max Plank Institute for Biogeochemistry, Hans-Knöll-Strasse 10, 07745 Jena, Germany
[5]Department of Global Ecology, Carnegie Institution for Science, Stanford, California 94305, USA
[6]Department of Biological Sciences, University of Cape Town, Rondebusch 7701, South Africa

ABSTRACT

The spacing of hills and valleys reflects the competition between disturbance-driven (or diffusive) transport on hillslopes and concentrative (or advective) transport in valleys, although the underlying lithologic, tectonic, and climatic controls have not been untangled. Here, we measure geochemical and geomorphic properties of catchments in Kruger National Park, South Africa, where granitic lithology and erosion rates are invariant, enabling us to evaluate how varying mean annual precipitation (MAP = 470 mm, 550 mm, and 730 mm) impacts hill-valley spacing or landscape dissection. Catchment-averaged erosion rates, based on ^{10}Be concentrations in river sands, are low (3–6 m/m.y.) and vary minimally across the three sites. Our lidar-derived slope-area analyses reveal that hillslopes in the dry site are gentle (3%) and short, such that the terrain is low relief and appears highly dissected. With increasing rainfall, hillslopes lengthen and increase in gradient (6%–8%), resulting in less-dissected, higher-relief catchments. The chemical depletion fraction of hilltop regoliths increases with rainfall, from 0.3 to 0.7, reflecting a climate-driven increase in chemical relative to physical erosion. Soil catenas also vary systematically with climate as we observe relatively uniform soil properties in the dry site that contrast with leached sandy crests and upper slopes coupled with downslope clay accumulation zones in the intermediate and wet sites. The geomorphic texture of this slow-eroding, granitic landscape appears to be set by climate-driven feedbacks among chemical weathering, regolith fabric differentiation, hydrological routing, and sediment transport that enhance the vigor of hillslope sediment transport relative to valley-forming processes for wetter climates.

INTRODUCTION

Eroding terrain has a remarkable tendency to organize into hill-valley sequences that collectively define drainage basins of varying scale. On hillslopes, sediment transport usually originates from disturbance-driven processes that tend to smooth the surface (Culling, 1965), whereas in valleys, fluid-driven transport drives localized incisions that connect to form channel networks. This simple but powerful framework suggests that the spacing of hills and valleys (and thus landscape dissection or drainage density) can be modeled as a competition between diffusive transport on hillslopes and advective transport in channels (e.g., Dunne and Aubry, 1986; Smith and Bretherton, 1972) although the specific mechanisms that regulate diffusive and advective fluxes likely vary with geologic and climate setting.

Globally, drainage density and relief vary by several orders of magnitude, but we lack models to predict how these characteristic scales depend on climate (Collins and Bras, 2010). Following earlier workers (see Simpson and Schlunegger [2003] for a review), Perron et al. (2009) developed a framework for assessing landscape dissection by quantifying how the relative magnitudes of hillslope and valley-forming processes control the spacing of hills and valleys in soil-mantled terrain. Their model separates hillslope transport and valley incision processes into diffusive (D) and advective (K) components, respectively. Their preliminary analysis suggests that wetter climates correspond with higher values of D/K and thus greater hill-valley spacing. While this proposed climate-geomorphic linkage is appealing, it has not been field tested in settings where the potentially confounding variables of erosion rate and bedrock lithology are held constant.

Here, we quantify climate control on topography in a post-orogenic landscape with uniform bedrock lithology and base-level control. In settings with low erosion rates, long regolith residence times support development of strongly weathered and highly differentiated regolith fabrics that modulate hillslope hydrology and sediment transport processes (Bishop, 2007). Our analysis combines lidar-derived morphologic trends for drainage density and local relief with estimates of total and chemical denudation to evaluate the role of climate in shaping granitic catchments of South Africa that span arid to sub-humid climates. Despite similar catchment-averaged erosion rates, our findings reveal profound differences in landscape morphology that reflect the key role of chemical weathering and regolith development in modulating hydrology and the relative efficacy of hillslope and valley-forming processes.

STUDY AREA: KRUGER NATIONAL PARK, SOUTH AFRICA

Over the last 90 m.y., the southern part of Africa has risen slowly in isostatic response to erosion (Tinker et al., 2008; Flowers and Schoene, 2010; Decker et al., 2013). Pliocene–Pleistocene rock uplift rates have been measured at 10–15 m/m.y. (Erlanger et al., 2012), consistent with minimal recent tectonic activity. Kruger National Park lies east of the Great Escarpment on the northeastern edge of South Africa bordering Mozambique (Fig. 1). The park stretches 350 km in a north-south orientation and is primarily underlain by Kaapvaal granite and metagranite in its western half (Venter, 1990) and Karoo volcanics in the eastern half. Rivers that traverse the study area are sourced on the escarpment and exhibit bedrock or mixed alluvial-bedrock beds. The eastern edge of the park is bounded by the Lebombo Mountains that are composed of resistant rhyolite that forms a base level regulating incision rates throughout the park (Venter, 1990).

Rainfall in Kruger primarily occurs in the austral summer and is controlled by onshore air flow associated with the warm Mozambique current as well as orographic effects that are in turn controlled by high topography along the Great Escarpment (Chase and Meadows, 2007). Climate in the park ranges from mildly arid in the north to sub-humid in the southwest where the park abuts the Great Escarpment (Fig. 1) (Gertenbach, 1980). Warmer temperatures in the north magnify this climate gradient by decreasing effective moisture. In the north, we sampled watersheds in the Phugwane River valley, which receives 470 mm of rain annually and has a mean annual air temperature (MAAT) of 23.1 °C (Venter et al., 2003). In the south, we sampled watersheds in the Nwaswitshaka River valley with 550 mm of rain annually and a MAAT of 21.9 °C, and in the Nsikazi River valley with 730 mm of rain annually and a MAAT

*E-mail: oac@geog.ucsb.edu.

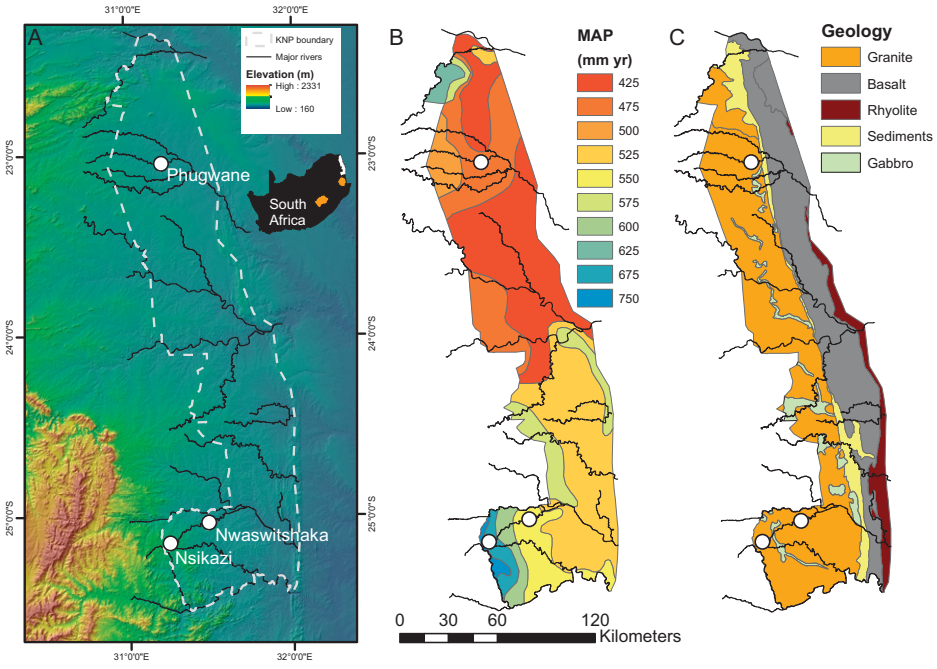

Figure 1. A: Shaded relief and elevation map showing boundary of Kruger National Park (KNP, South Africa), edge of Great Escarpment in the west, Lebombo Mountains (slight ridge along eastern edge of park), and rivers where erosion rates were measured. B: Mean annual rainfall (MAP) map. C: Geologic map. Catchment sampling sites are shown as white circles on each graphic.

of 21.6 °C (Fig. 1) (Venter et al., 2003). Evidence suggests that the rainfall gradient, which derives from an Indian Ocean source for atmospheric moisture and orographic control, has been a consistent feature for millions of years (see the GSA Data Repository[1]).

Regoliths (soil and saprolite) in the park are dominated by ~60-cm-thick Aridisols in the northern arid zone, ~100-cm-thick Inceptisols and Alfisols in the semi-arid zone, and ~200-cm-thick, highly weathered Inceptisols and Alfisols in the sub-humid zone (Khomo et al., 2011). With increasing rainfall, hillslope regolith fabric becomes strongly differentiated into highly leached and collapsed, but porous, ridge crests and upper side slopes that contrast with lower side slopes that are packed with low-permeability clays translocated from upslope (Khomo et al., 2013; Bern et al., 2011) (Fig. DR1 in the Data Repository). In the site with 550 mm of rainfall, the upper edge of the clay-rich zone occurs about halfway between hillcrests and channel margins, whereas in the site with 730 mm of rainfall, it occurs along the lower 20% of most slopes. Within each rainfall zone, these soil-hillslope patterns are spatially consistent as revealed by distinctive patterns of vegetation and termite mounds (Levick et al., 2010). In the intermediate and wet sites, the clay accumulation zones control seasonal seep lines along the contour defined by the upper edge of the clay accumulation zone. The seeps are created by subsurface flow returning to the surface where it can produce gullies and soil slips that deliver sediment from near-stream positions into the valley network (Venter, 1990). By contrast, catenas in the site with 470 mm of rainfall exhibit less clay redistribution and more evidence of dispersive overland flow and sheetwash.

METHODS

We estimated long-term erosion rates by measuring ^{10}Be concentrations in the quartz fraction of river channel sediments (Table DR1). In each climate zone, we sampled first- to fourth-order catchments within the Kaapvaal granite to minimize differences in bedrock erodibility. The broadly convex soil-mantled hillslopes do not evidence deep-seated landsliding or other processes that could preferentially contribute sediment from depths below the attenuation length of cosmic rays. Because cosmogenic nuclides accumulate over thousands of years, they are unaffected by any recent land-use changes and are also insensitive to changes in sediment storage given that storage area is negligible relative to total catchment area at our sites. We characterized the weathering status of ridge-crest regoliths by estimating the depth-averaged chemical depletion fraction (CDF) referenced to local rock (Riebe et al., 2004), which represents the portion of denudation that is achieved through chemical means. Particularly for the intermediate and wet sites, we note that the CDF value depends on hillslope position relative to the clay accumulation zone (Khomo et al., 2013). We did not correct the catchment-averaged erosion rates for the weathering status of bounding hillslopes (e.g., Riebe and Granger, 2013) because the complex nature of the catenas would require accounting for the areal distribution of differing weathering profiles.

We used slope-area plots to characterize morphologic trends, including variations in hillvalley spacing and local relief. These plots are diagnostic because they describe how the local gradient increases downslope from hilltops and reaches a maximum before decreasing downstream in the valley network (Fig. DR2). The drainage area where the convex hillslope and concave valley trends intersect (denoted here as A_{HV}) serves as an objective proxy for the average hill-valley spacing or drainage density (Roering et al., 2007; Collins and Bras, 2010) (Fig. DR3). We acquired airborne lidar data for large swaths of terrain in each of the three climate zones using the Carnegie Airborne Observatory (http://cao.ciw.edu) and generated bare-earth digital elevation models (DEMs) with a 1.12 m grid spacing (Asner et al., 2007). We digitally excised ~2-m-high termite mounds and other ephemeral roughness features by performing a wavelet transformation with an ~16 m Mexican hat wavelet and removing nodes with a correlation value greater than 8. We filled in the "no data" nodes and smoothed the topography by fitting a second-order weighted polynomial to a 25 × 25 node array of neighboring points, following Wood (1996). The fitting algorithm outputs include a smoothed elevation value at each grid node as well as polynomial coefficients used to calculate topographic derivatives, including local gradient. We used the D-infinity multi-direction flow routing algorithm to calculate drainage area for every node on the smoothed DEMs (Tarboton, 1997).

RESULTS

Catchment-averaged erosion rates are low (Fig. 2A) and consistent with values typical of post-orogenic landscapes worldwide, particularly those measured in southern Africa (Decker et al., 2013; Flowers and Schoene, 2010). Specifically, erosion rates across first- to fourth-order streams average 5.9 ± 0.7 m/m.y. at the 470-mm-rainfall site, 6.6 ± 1.0 m/m.y. at the 550-mm-rainfall site, and 4.0 ± 0.8 m/m.y. at the 730-mm-rainfall site. Within-site erosion rate variation does not depend on stream order (Table DR1). Between-site variation is minimal and may be attributable to non-quantified factors, such as minor local bedrock-controlled knickpoints and the influence of hillslope weathering

[1]GSA Data Repository item 2013326, paleoclimate information, catena weathering properties, ^{10}Be data table, slope-area plot explanatory figures, graph of bare earth quantity for sampling sites, and photograph of soil slips in lower part of wet catena, is available online at www.geosociety.org/pubs/ft2013.htm, or on request from editing@geosociety.org or Documents Secretary, GSA, P.O. Box 9140, Boulder, CO 80301, USA.

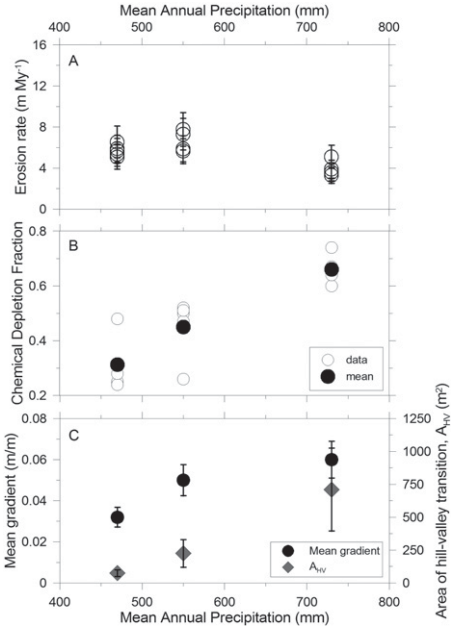

Figure 2. Plot of variations in erosion rate (A), chemical depletion fraction (B), and mean hillslope gradient and drainage area of the hill-valley transition (A_{HV}) (C) with annual precipitation for our three study sites. Erosion rates do not exhibit systematic variations with precipitation, whereas the chemical depletion fraction, mean gradient, and A_{HV} increase with annual precipitation.

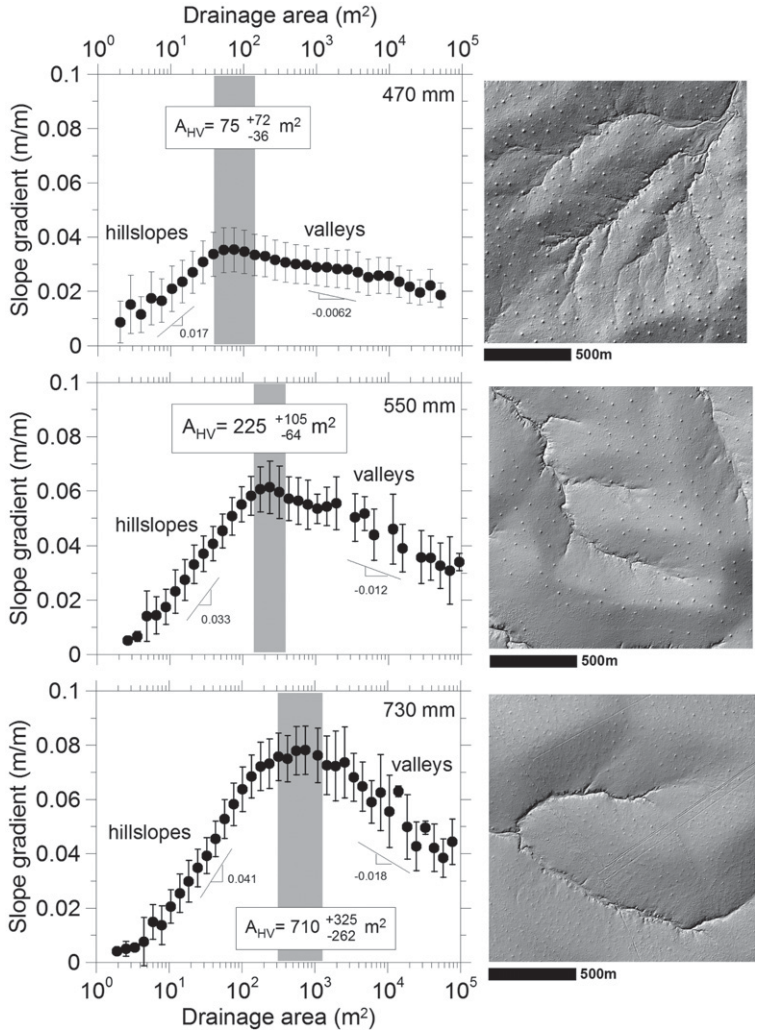

Figure 3. Slope-area plots for 1.5 × 1.5 km patches of terrain in each of the three climate zones (see Fig. DR4 [see footnote 1]). Drainage area of hillslope-valley transition (shaded vertical band) increases with mean annual precipitation (noted in upper right corner of each plot). Slope symbols in lower part of each plot refer to average convexity for hillslopes and concavity for valleys, and have units of gradient/log(area). Error bars represent one standard deviation of slope for each log bin of drainage area. Width of shaded bar approximates standard error of hillslope gradient and drainage area of hill-valley transition (A_{HV}) estimate, and is derived from uncertainty analysis of a spline fit to the binned area-slope curve.

status on stream sediment ^{10}Be concentrations (cf. Riebe and Granger, 2013). Despite similar erosion rates, mean CDF values for hillcrest regoliths increased from 0.3 to nearly 0.7 with increasing rainfall (Fig. 2B). This pattern implies a considerable shift from physically dominated erosion in dry catchments to chemically dominated erosion in wet catchments, and corresponds with a thickening of regolith with rainfall (Khomo et al., 2011, 2013). Using average regolith depth and catchment-averaged erosion rate estimates, we infer long hillcrest regolith residence times of 0.11, 0.15, and 0.57 m.y. for the dry, intermediate, and wet sites, respectively.

We averaged slope-area data for representative 1.5 × 1.5 km patches of terrain in each of the three rainfall zones (Fig. DR4) and estimated the average drainage area associated with the hill-valley transition, or A_{HV} (Fig. 2C). Within each rainfall zone, we observed characteristic convex hillslope and concave valley morphologic trends (Fig. 3). Values of hillslope convexity (defined here by the rate of slope increase with the log of upslope area) and valley concavity (the rate of slope decline with the log of upslope area) are lower for the dry site than for the intermediate and wet sites, reflecting lower hillslope and catchment relief. More importantly, the value of A_{HV} revealed by our slope-area analysis increases monotonically with rainfall, such that wetter conditions promote broader hillslopes, increased local relief, and lower drainage density (Fig. 2C).

DISCUSSION AND CONCLUSIONS

The topographic form of granitic hill-valley terrain in Kruger National Park can be approximated using a diffusion-advection model framework. The observation that hill-valley spacing and local relief increase with annual rainfall given constant rock type and erosion rate suggests that wetter climates increase the efficacy of hillslope transport relative to fluvial action. Below, we suggest that over the long regolith residence times associated with this post-orogenic landscape, the diffusive transport component may be partitioned differently into solute and particulate fluxes depending on climate controls on plant cover, overland flow, bioturbation, infiltration and throughflow, and the fate of weathering products.

The relative simplicity of the diffusion-advection framework, however, belies the spectrum of processes that serve as diffusive or advective transport mechanisms and thus facilitate this morphologic pattern in our study area. Field observations reveal different sediment transport mechanisms in the different climatic settings. At the dry site, rain-splash and intermittent slope-wash processes dominate hillslope fluxes due to the relatively sparse vegetative cover (quantified as bare earth in Fig. DR5) and local concentrations of fine-grained particles associated with numerous termite mounds. Along these hillslopes, we observe pebble lags indicative of intermittent and discontinuous overland-flow erosion. At wetter sites, more extensive vegetative cover favors transport via bioturbation, including burrowing and tree turnover as evidenced by overturned root wads and localized collections

of coarse bedrock clasts on the surface. In these sites, long-term water flux has transported chemical-weathering products downslope forming strongly differentiated catenas comprising highly permeable sandy crests and clay-rich lower-slope regoliths (Bern et al., 2011; Khomo et al., 2011, 2013; Fig. DR1). We suggest that differences in hydrological partitioning, which dictates transport mechanisms, among the three sites provide an important mechanism by which climate modulates hillslope-channel coupling and thus catchment morphology.

Our analysis of climate controls on hillslope-channel morphology assumes minimal transient response to perturbations in climatic or tectonic forcing. Given slow rock uplift rates and a persistent control on base-level lowering, the observed landform patterns must have persisted for millions of years, suggesting relatively steady-state conditions. This interpretation is supported by models of transient hillslope response, which suggest that hillslopes of the scale observed here require ~10^6 yr to adjust to changing boundary conditions (Mudd and Furbish, 2007), which is much less than the time since tectonic and climate conditions stabilized. More so, the erosion rates estimated here suggest that total denudation since the late Mesozoic has exceeded 100 m, which is more than four times the typical relief (~20 m), further lending support for an interpretation of steady-state conditions (Howard, 1994).

Despite ample support for relatively uniform erosion rates, our analyses have yet to reconcile the differentiated catena properties described here with an interpretation of steady-state conditions. Steady erosion requires that clay accumulation zones be maintained at their present positions through replenishment from upslope and physical denudation along their lower margins. Alternatively, a non-steady scenario would predict that clay accumulation zones are propagating upslope or downslope. We do not observe evidence of such a transient response, however, because for a given climate condition, the relative location of clay concentrations and seep lines is remarkably consistent (Levick et al., 2010). In the field, we do observe clay-zone erosion by ephemeral gully formation and soil slips (Fig. DR6), although these processes only locally disturb the clay-rich zone. Thus, conditions on Kruger hillslopes appear to approximate steady-state denudation while experiencing small-scale transient responses due to late Cenozoic climate change and/or autogenic variability.

In our post-orogenic study area with constant erosion rate and lithology, wetter climate conditions increase the vigor of hillslope processes relative to valley-forming ones. This occurs across the transition from relatively infrequent and short-lived overland events in the dry site to throughflow-dominated hydrologic response and enhanced bioturbation in the wetter sites. The increasing relative importance of hillslope processes under wetter climates is influenced by the weathering (and thus residence time) of regolith, given that catena fabric differentiation modulates hydrology and sediment transport. More generally, the interplay between chemical and physical denudation observed on hillslopes in this slowly eroding landscape is subject to feedbacks involving climate, vegetation, hydrology, and regolith development that have yet to be codified in theoretical landscape evolution models.

ACKNOWLEDGMENTS

We thank the Carnegie Airborne Observatory (CAO) team and A. Booth for lidar data collection, processing, and DEM modeling. Roering was supported by National Science Foundation grant EAR-0952186, and the rest of the authors were supported by the Andrew Mellon Foundation. The CAO was funded by the Gordon and Betty Moore Foundation, the Grantham Foundation for the Protection of the Environment, Avatar Alliance Foundation, W.M. Keck Foundation, the Margaret A. Cargill Foundation, Mary Anne Nyburg Baker and G. Leonard Baker Jr., and William R. Hearst III.

REFERENCES CITED

Asner, G.P., Knapp, D.E., Kennedy-Bowdoin, T., Jones, M.O., Martin, R.E., Boardman, J., and Field, C.B., 2007, Carnegie Airborne Observatory: In-flight fusion of hyperspectral imaging and waveform light detection and ranging for three-dimensional studies of ecosystems: Journal of Applied Remote Sensing, v. 1, 013536, doi:10.1117/1.2794018.

Bern, C.R., Chadwick, O.A., Hartshorn, A.S., Khomo, L.M., and Chorover, J., 2011, A mass-balance model to separate and quantify colloidal and solute redistributions: Chemical Geology, v. 282, p. 113–119, doi:10.1016/j.chemgeo.2011.01.014.

Bishop, P., 2007, Long-term landscape evolution: Linking tectonics and surface processes: Earth Surface Processes and Landforms, v. 32, p. 329–365, doi:10.1002/esp.1493.

Chase, B.M., and Meadows, M.E., 2007, Late Quaternary dynamics of southern Africa's winter rainfall zone: Earth-Science Reviews, v. 84, p. 103–138, doi:10.1016/j.earscirev.2007.06.002.

Collins, D.B.G., and Bras, R.L., 2010, Climatic and ecological controls of equilibrium drainage density, relief, and channel concavity in dry lands: Water Resources Research, v. 46, W04508, doi:10.1029/2009WR008615.

Culling, W., 1965, Theory of erosion on soil-covered slopes: The Journal of Geology, v. 73, p. 230–254.

Decker, J.E., Niedermann, S., and de Wit, M.J., 2013, Climatically influenced denudation rates of the southern African plateau: Clues to solving a geomorphic paradox: Geomorphology, v. 190, p. 48–60, doi:10.1016/j.geomorph.2013.02.007.

Dunne, T., and Aubry, B.F., 1986, Evaluation of Horton's theory of sheetwash and rill erosion on the basis of field experiments, *in* Abrahams, A.D. ed., Hillslope Processes: London, Allen and Unwin, p. 31–53.

Erlanger, E.D., Granger, D.E., and Gibbon, R.J., 2012, Rock uplift rates in South Africa from isochron burial dating of fluvial and marine terraces: Geology, v. 40, p. 1019–1022, doi:10.1130/G33172.1.

Flowers, R.M., and Schoene, B., 2010, (U-Th)/He thermochronometry constraints on unroofing of the eastern Kaapvaal craton and significance for uplift of the southern African Plateau: Geology, v. 38, p. 827–830, doi:10.1130/G30980.1.

Gertenbach, W.P.D., 1980, Rainfall patterns in the Kruger National Park: Koedoe, v. 25, p. 35–43.

Howard, A.D., 1994, A detachment-limited model of drainage basin evolution: Water Resources Research, v. 30, p. 2261–2285, doi:10.1029/94WR00757.

Khomo, L., Hartshorn, A.S., Rogers, K.H., and Chadwick, O.A., 2011, Impact of rainfall and topography on the distribution of clays and major cations in granitic catenas in southern Africa: Catena, v. 87, p. 119–128, doi:10.1016/j.catena.2011.05.017.

Khomo, L., Bern, C.R., Hartshorn, A.S., Rogers, K.H., and Chadwick, O.A., 2013, Chemical transfers along slowly eroding catenas developed on granitic cratons in southern Africa: Geoderma, v. 202–203, p. 192–202, doi:10.1016/j.geoderma.2013.03.023.

Levick, S.R., Asner, G.P., Chadwick, O.A., Khomo, L.M., Rogers, K.H., Hartshorn, A.S., and Knapp, D.E., 2010, Regional insight into savanna hydrogeomorphology from termite mounds: Nature Communications, v. 1, no. 6, p. 1–7, doi:10.1038/ncomms1066.

Mudd, S.M., and Furbish, D.J., 2007, Responses of soil-mantled hillslopes to transient channel incision rates: Journal of Geophysical Research, v. 112, F03S18, doi:10.1029/2006JF000516.

Perron, J.T., Kirchner, J.W., and Dietrich, W.E., 2009, Formation of evenly spaced ridges and valleys: Nature, v. 460, p. 502–505, doi:10.1038/nature08174.

Riebe, C.S., and Granger, D.E., 2013, Quantifying effects of deep and near-surface chemical erosion on cosmogenic nuclides in soils, saprolite, and sediment: Earth Surface Processes and Landforms, v. 38, p. 523–533, doi:10.1002/esp.3339.

Riebe, C.S., Kirchner, J.W., and Finkel, R.C., 2004, Erosional and climatic effects on long-term chemical weathering rates in granitic landscapes spanning diverse climate regimes: Earth and Planetary Science Letters, v. 224, p. 547–562, doi:10.1016/j.epsl.2004.05.019.

Roering, J.J., Perron, J.T., and Kirchner, J.W., 2007, Functional relationships between denudation and hillslope form and relief: Earth and Planetary Science Letters, v. 264, p. 245–258, doi:10.1016/j.epsl.2007.09.035.

Simpson, G., and Schlunegger, F., 2003, Topographic evolution and morphology of surfaces evolving in response to coupled fluvial and hillslope sediment transport: Journal of Geophysical Research, v. 108, 2300, doi:10.1029/2002JB002162.

Smith, T.R., and Bretherton, F.P., 1972, Stability and the conservation of mass in drainage basin evolution: Water Resources Research, v. 8, p. 1506–1529, doi:10.1029/WR008i006p01506.

Tarboton, D.G., 1997, A new method for the determination of flow directions and upslope areas in grid digital elevation models: Water Resources Research, v. 33, p. 309–319, doi:10.1029/96WR03137.

Tinker, J., de Wit, M., and Brown, R., 2008, Linking source and sink: Evaluating the balance between onshore erosion and offshore sediment accumulation since Gondwana break-up, South Africa: Tectonophysics, v. 455, p. 94–103, doi:10.1016/j.tecto.2007.11.040.

Venter, F.J., 1990, A classification of land for management planning in the Kruger National Park [Ph.D. thesis]: Pretoria, University of South Africa, 392 p.

Venter, F.J., Scholes, R.J., and Eckhardt, H.C., 2003, The abiotic template and its associated vegetation pattern, *in* Du Toit, J.T, Rogers, K.H., and Biggs, H., eds., The Kruger Experience: Ecology and Management of Savanna Heterogeneity: Washington, D.C., Island Press, p. 83–129.

Wood, J., 1996, The geomorphological characterization of digital elevation models [Ph.D. thesis]: Leicester, UK, University of Leicester, 102 p.

Manuscript received 8 May 2013
Revised manuscript received 28 July 2013
Manuscript accepted 29 July 2013

Printed in USA

Data Repository/Supplementary Materials: Shaping post-orogenic landscapes by climate and chemical weathering, Chadwick et al.

Paleoclimate Approximately 30 Mya, drying of Southern Africa occurred due to enhancement of the circum-Antarctic Polar Current and this pattern has persisted to the present (Chase and Meadows, 2007). In the Pleistocene, moisture and temperature fluctuations in the region have occurred due to changing sea-surface temperatures, the incursion of westerly storms into the continental interior due to expanding Antarctic sea ice, and changes in the extent of the Inter-Tropical convergence zone to the north of our study area (Chase and Meadows, 2007; Gasse et al., 2008). The collective influence of these Quaternary fluctuations on climate in southern Africa in the vicinity of Kruger appears to have influenced effective moisture by 20% or less as evidenced by paleo-environmental reconstructions over the last 200 ky in the Pretoria pan (Partridge et al., 2003). In summary, it appears that our study area has not been subject to profound variations in tectonic or climatic forcing in the last 30 Mya and perhaps longer.

Regolith Properties Along Catenas

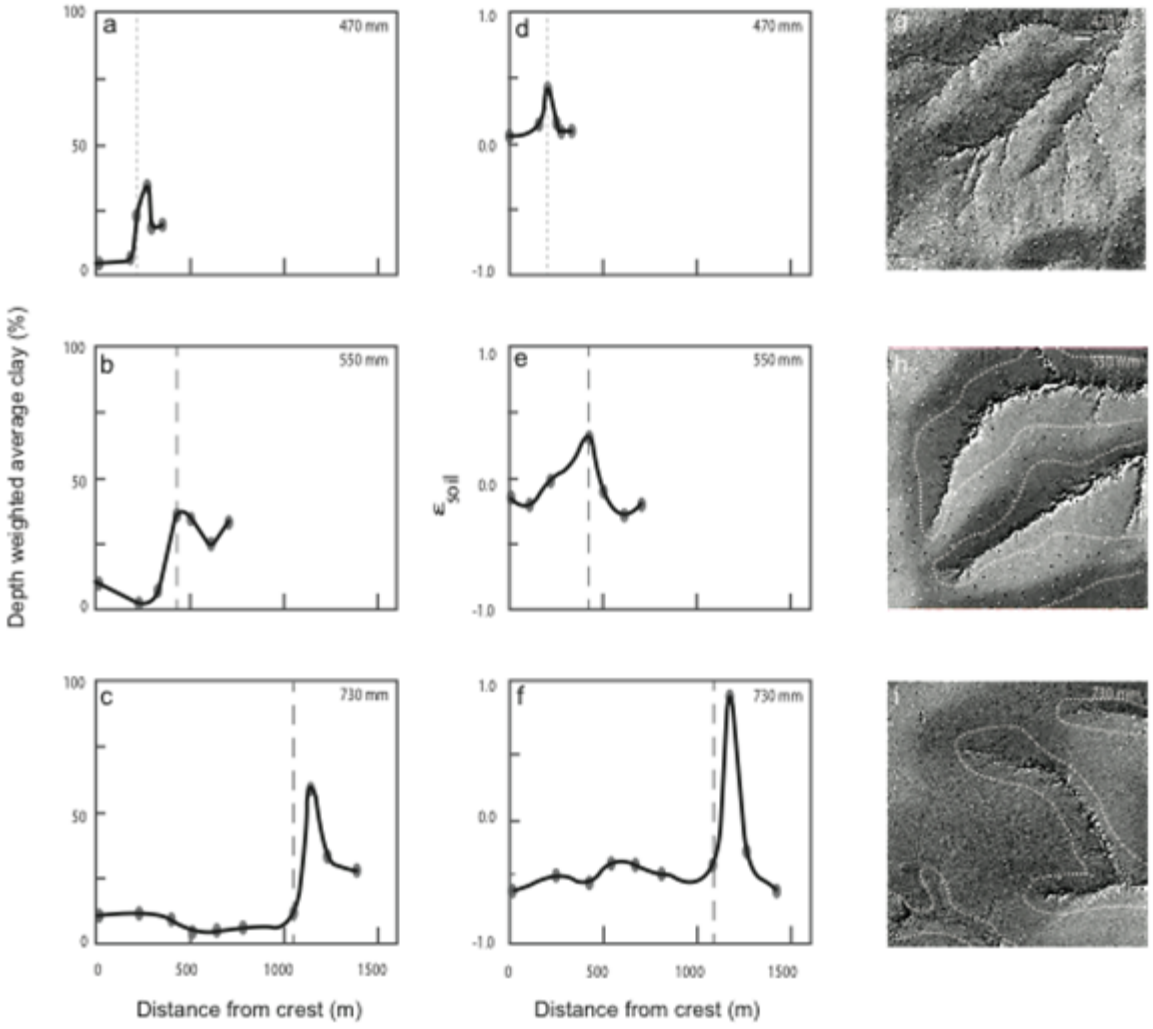

Figure DR1. Clay accumulation in regoliths as a function of distance along catenas (A-C), its impact on profile dilation or collapse (D-F) and the geographic location of seeplines developed at the contact between sandy, highly permeable soils upslope and clay-rich, low permeability soils downslope (dashed lines on G-I). Clay data are depth-weighted average values from surface to hard rock in the dry site and from surface to saprolite contact for the wetter sites and are derived from data presented in Khomo et al., (2011). Soil strain data ($\varepsilon_{i,w} = ((\rho_p C_{i,p})/(\rho_w C_{i,w}))-1$ where ρ is bulk density, C_i is an immobile element concentration (Zr) and the subscripts p and w represent values for rock and regolith, respectively (Brimhall et al., 1992)) are based on density and Zr data from the same soil profiles as those shown in column one (see Khomo et al., 2013). When $\varepsilon_{i,w}$ is <0 collapse is indicated. The seepline (hydrological expression of the sand-to-clay transition) shown as vertical dashed lines in A-F are based on field observations of soil wetness and redoxymorphic features whereas the landscape distribution of seeplines in G-I is shown as dashed lines and determined by a spatial analysis of vegetation and termite mound distributions that are sensitive to clay concentration and water saturation

presented in Levick et al. (2010). Clay accumulation is mediated by through-regolith water flux and hence by effective moisture. In the arid zone, clay redistribution is negligible because overland flow and high evapotranspiration greatly reduces throughflow in soils (Khomo et al., 2011; Bern et al., 2011). As a consequence evidence for a seepline at the sand-to-clay contact exists within soil as redoxymorphic features but cannot be determined as a specific landscape feature (seepline shown as dotted line on A and D, but no seepline shown on G). In the arid catenas dilation of the catena profiles is likely driven by dust inputs whereas in the wetter sites weathering dominates generating collapse at the crests and dilation in parts of the clay-rich zone (Khomo et al., 2013).

Catchment Average Erosion Rates

We measured ^{10}Be concentrations in quartz-rich sediments in 1st through 4th order watersheds (as defined by Strahler, 1957) ranging in size from <1 to >750 km^2 (Table DR1) to determine catchment-averaged erosion rates (Brown et al., 1995; Granger et al., 1996; Bierman and Steig, 1996). This method has been successfully applied in numerous studies of upland landscapes (e.g., von Blanckenburg, 2005 and references within). For each catchment, we separated quartz using standard techniques (Kohl and Nishiizumi, 1992) while PrimeLab (Purdue University) performed the ^{10}Be isolation and measurement. We calculated ^{10}Be production rates for each catchment, correcting for elevation and latitude (Dunai, 2000). Topographic shielding and muogenic production were not accounted for, and contribute to an estimated 5% uncertainty in production rates that is added to the 1σ analytical error. Although we did not quantify the impact of catchment weathering status and quartz content on catchment-averaged erosion rates, we do not expect significant variation as all of the basins sample quartz-rich granitic rocks and the regolith does not have thick saprolite layers, which might skew average catchment erosion rates significantly (Riebe and Granger, 2013).

TABLE DR1: AVERAGE EROSION RATES FROM COSMOGENIC BE-10 CONCENTRATIONS

Sample	Weight (g)	Carrier (µg)	Latitude (DD)	Longitude (DD)	Avg. Elev. (m)	Stream Order	Area (km^2)	[Be-10] atoms g^{-1}	error	E (m Ma^{-1})	error
Arid Catchments											
KR-15	30.291	0.300	-23.047	31.229	324	1	0.034	572960	19352	5.90	0.65
KR-16	30.536	0.301	-23.046	31.230	345	1	0.059	598771	11727	5.70	0.60
KR-17	30.186	0.300	-23.044	31.235	346	2	0.605	531510	28449	6.55	0.78
KR-18	30.431	0.301	-23.043	31.243	323	3	10.291	620945	17978	5.36	0.59
KR-19	30.557	0.301	-23.124	31.289	403	4	757.837	687701	29690	5.07	0.59
KR-114	23.113	0.307	-23.037	31.280	400	4	---	538950	12400	6.72	0.70
Semi-Arid Catchments											
KR-1	30.848	0.301	-25.025	31.495	350	1	0.043	493396	14951	7.30	0.77
KR-2	30.248	0.301	-25.020	31.491	355	2	0.478	469055	14528	7.76	0.82
KR-4	30.123	0.299	-25.037	31.504	433	4	138.023	628558	15957	5.88	0.63
KR-5	30.418	0.300	-25.030	31.502	352	3	1.711	614836	13801	5.66	0.61
Sub-Humid Catchments											
KR-6	30.237	0.301	-25.212	31.282	563	1	0.281	975502	16819	3.90	0.44
KR-7	30.405	0.303	-25.222	31.272	586	3	35.127	1063104	17543	3.59	0.41
KR-8	30.065	0.302	-25.220	31.273	555	2	8.573	1110870	20532	3.31	0.39
KR-11	30.093	0.299	-25.236	31.267	573	4	58.755	780108	16034	5.11	0.56

Concentration errors include 1 σ from AMS. All errors propagated to average erosion rates.

Latitude and altitude production rate scaling factor used pixel-pixel for catchment-averaged rates (Dunai, 2000).

Densities: Sediment, 2.6 g cm^{-3}, for *Avg. E*; lambda 145 g cm^{-2}.

^{10}Be from rescaled sea level production rate of and 5.1 atoms g^{-1} yr^{-1} (Balco et al., 2008).

^{10}Be ratios calibrated to 07KNSTD, measured at PRIME lab AMS

Stream order based on Strahler (1957) classification.

Area-slope transition as a proxy for ridge-valley spacing and landscape dissection

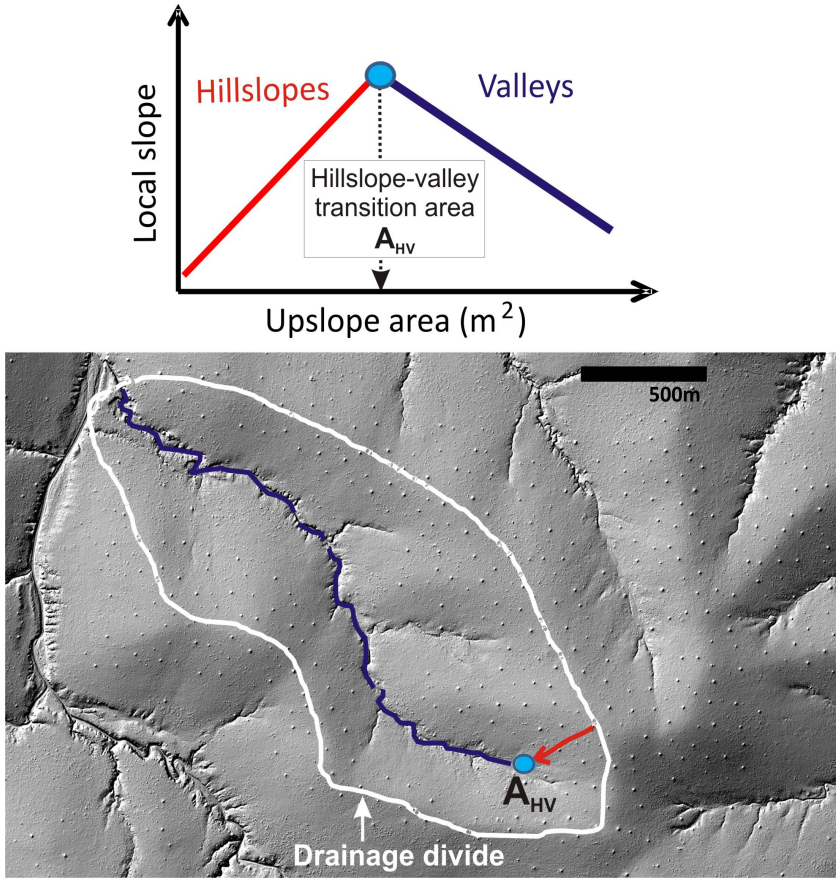

Figure DR2. Schematic of area-slope plot and corresponding location of hillslope, transition area, and valley network on a shaded relief image from our intermediate rainfall site. Slope increases downslope on hillslopes (red line) before reaching a maximum near the area of the hillslope-valley ($\mathbf{A_{HV}}$), which is shown by a light blue filled circle. At larger drainage areas, local slope decreases reflecting the tendency for channel profiles to be concave (i.e., become gentler downstream). Note that the hillslope-valley transition area is an average value and will vary within a given setting due to natural variations as well as uncertainty in the flow routing algorithm used. Importantly, our area-slope analysis averages all possible flowpaths within a 1.5km x 1.5km area (shown in Figure DR4) for each climate zone to arrive at the characteristic values of $\mathbf{A_{HV}}$, which is a proxy for ridge-valley spacing and landscape dissection. Higher values of $\mathbf{A_{HV}}$ correspond to larger ridge-valley spacing and lower valley density.

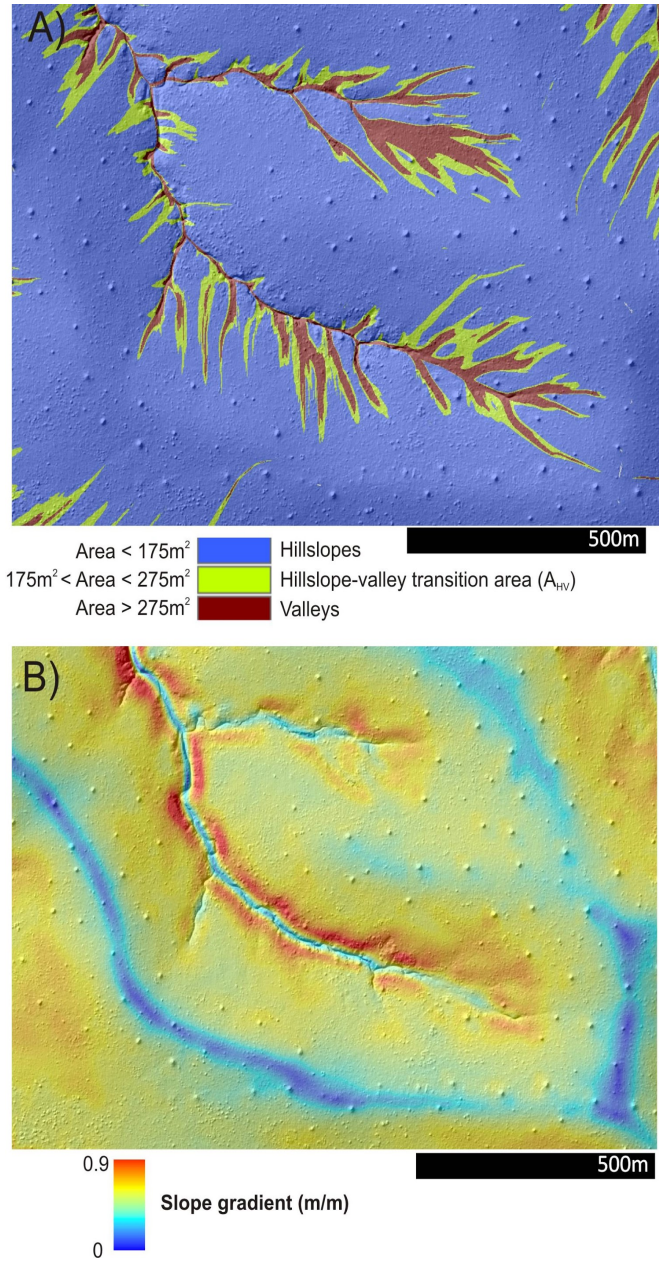

Figure DR3. Example maps of drainage area (A) and local slope (B) for a small catchment in our intermediate rainfall study site. **A)** Note that hillslopes have low drainage area (blue) and comprise the vast majority of the landscape. The transition between hillslopes and valleys at drainage areas between 175 and 275 m^2 is demarcated in yellowish-green. We averaged the areal extent of this transition for each climatic zone in our study area. Variability in the hillslope-valley transition area (A_{HV}) is apparent in A, but is not significant relative to the differences in A_{HV} that we observe amongst our study sites. Where the transition area (i.e., yellow areas) transgresses onto hillslopes, we often observe subtle, unchanneled depressions that may reflect transient adjustment to valley network dynamics. In other words, the tips of the valley network appear to be dynamic. **B)** Slope gradient for the same catchment

shown in B. Note that hilltops are gentle and hillslopes increase in steepness in the downslope direction (which defines a convex form) and tend to be steepest near the hillslope-valley transition. Because our wavelet filter effectively removes termite mounds before we smooth the topography, these 2m-high features do not influence local slope or flowpaths.

Figure DR4. Shaded relief images used for slope-area analysis (red boxes are 1.5km x 1.5km). Within each box, all data was averaged to generate relationships illustrated in Fig. 3 in the text.

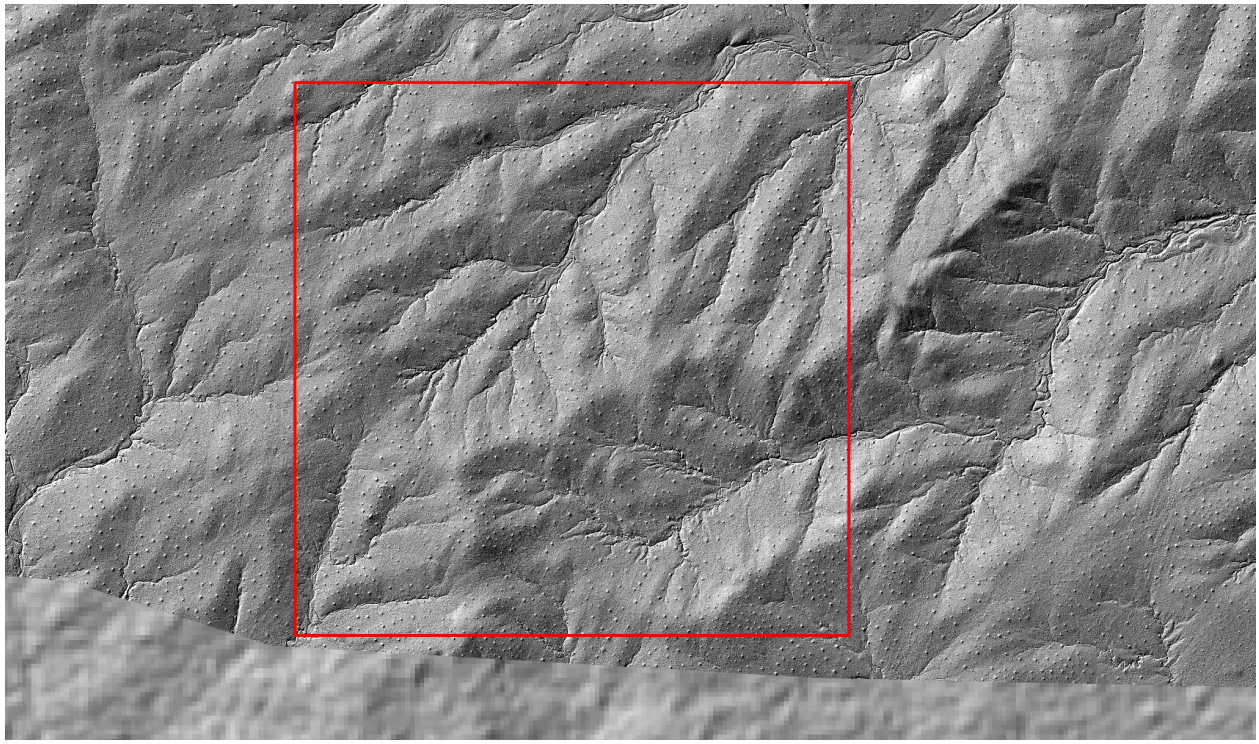

A) Phugwane area (Mean Annual Precipitation = 470 mm, lat/long: -22.999, 31.187)

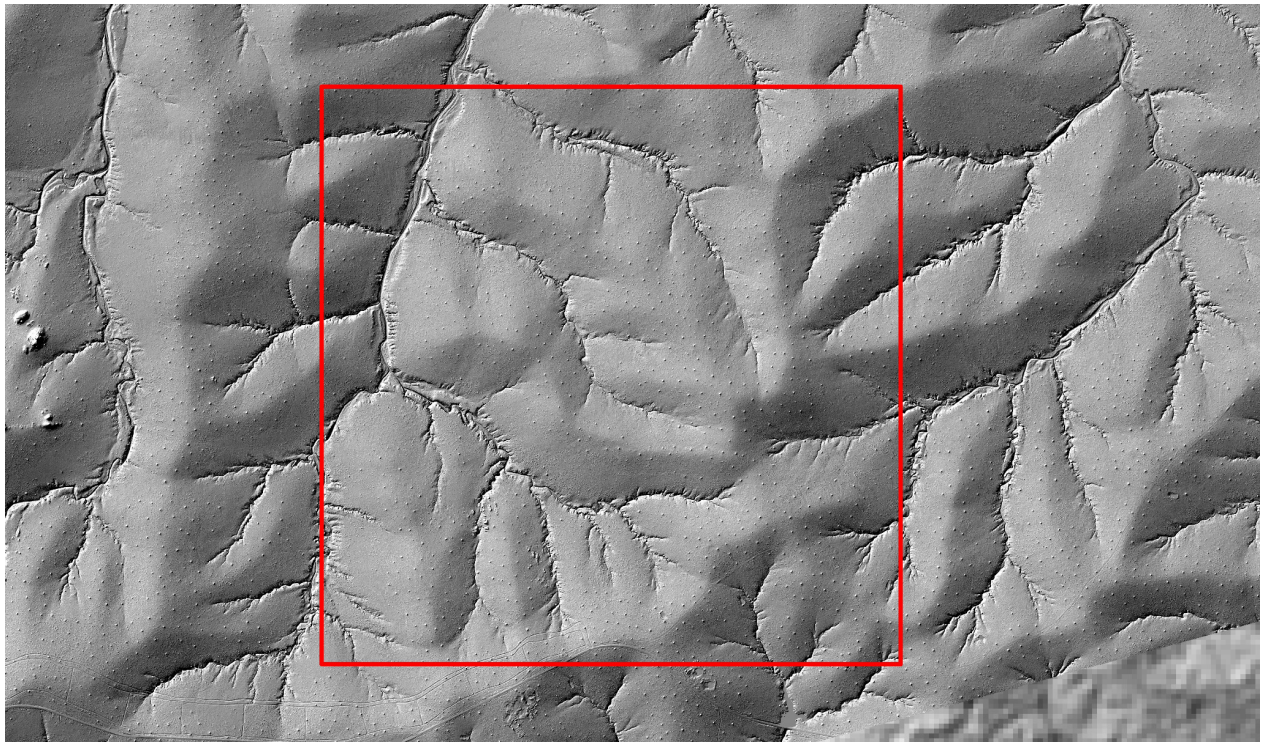

B) Skukuza area (Mean Annual Precipitation = 550 mm, lat/long: -25.082, 31.472)

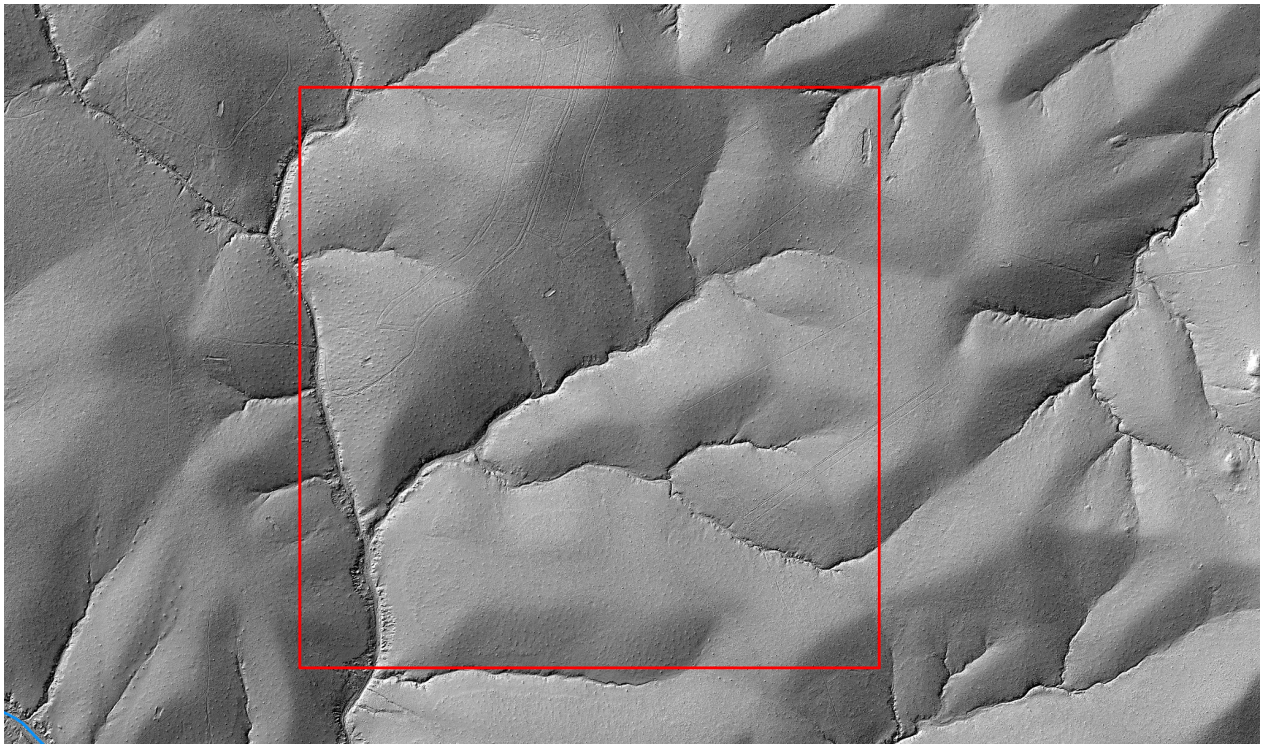

C) Pretoriuskop area (Mean Annual Precipitation = 730 mm, lat/long: -25.213, 31.287)

Quantification of Bare Ground

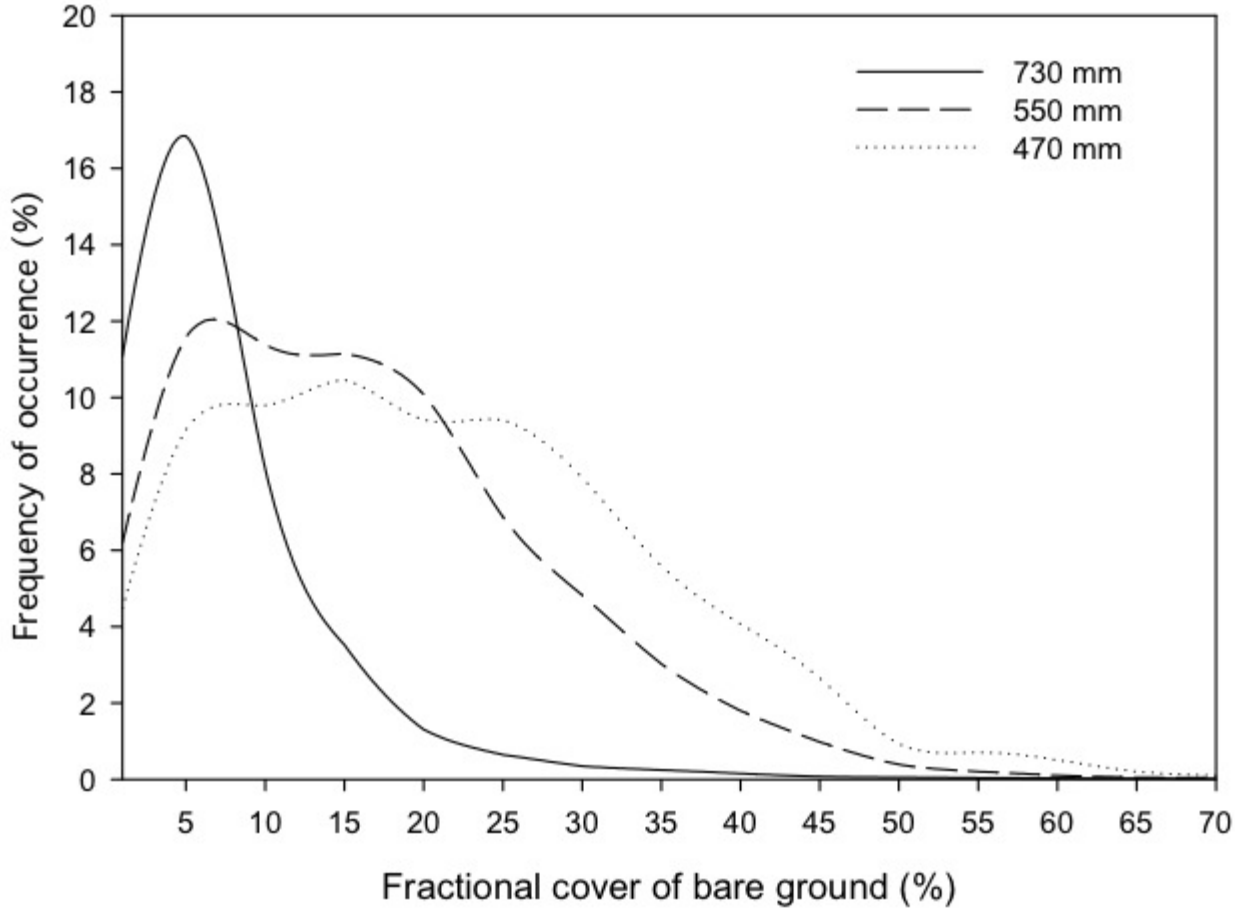

Figure DR5. Frequency distribution of bare ground for a 4.8 ha area in each rainfall zone. The area was imaged using the CAO hyperspectral instrument producing 5 m pixels. Bare ground data were separated from photosynthetic vegetation and non-photosynthetic vegetation using a pixel unmixing algorithms. Mean values for bare ground are 16.2, 9.8 and 3.7%, respectively for the 470, 550 and 730 mm rainfall sites. Data and methods are presented in Asner et al. (2009).

Hotspots of Erosion Near the Lower End of Catenas

Figure DR6. Example of soil slip near the lower edge of the clay-rich zone in the wet site near area shown in Supplementary Fig. 1, I. The channel that evacuates the local catena sediments from the catchment is located in the lower right part of the picture. The upper edge of the soil slip is about 100 m from the channel. Erosion features like this are not found higher in the landscape except where roads have artificially concentrated flow. Oblique photo taken from helicopter by Shaun Levick.

References Cited for Supplementary Materials

Asner, G. P., Levick, S. R., Kennedy-Bowdoin, T., Knapp, D.E., Emerson, R. Jacobson, J., Colgan, M. S., and Martin, R. E., 2009, Large-scale impacts of herbivores on the structural diversity of African savannas: Proceedings of the National Academy of Sciences, v. 106, p. 4947-4952.

Bern, C.R., Chadwick, O.A., Hartshorn, A.S., Khomo, L.M., and Chorover, J., 2011, A mass balance model to separate and quantify colloidal and solute redistributions: Chemical Geology v.282, p. 113–119.

Bierman, P., & Steig, E.J., 1996, Estimating rates of denudation using cosmogenic isotope abundances in sediment: Earth Surf. Processes and Landforms v. 21, P. 125–139.

Brimhall, G.H, Chadwick, O.A., Lewis, C.J., Compston, W., Dietrich, W.E., Powers, M., Hendricks, D.M., and Bratt, J., 1992, Deformational mass transport and invasive processes in soil evolution: Science, v. 255, p. 695-702.

Brown, E.T., Stallard, R.F., Larsen, M.C., Raisbeck, G.M., and Yiou, F., 1995, Denudation rates determined from the accumulation of in situ-produced 10Be in the Luquillo Experimental Forest, Puerto Rico: Earth Planet. Sci. Lett. v.129, p. 193–202.

Chase, B. M., & Meadows, M. E., 2007, Late Quaternary dynamics of southern Africa's winter rainfall zone: Earth-Science Reviews, v. 84, p. 103-138.

Dunai, T.J., 2000, Scaling factors for production rates of in situ produced cosmogenic nuclides: a critical reevaluation: Earth Planet. Sci. Lett. v.176, p. 157–169.

Gasse, F., Chalie, F., Vinces, A., Williams, M.A.J., and Williamson, D., 2008, Climatic patterns in equatorial and southern Africa from 30,000 to 10,000 years ago reconstructed from terrestrial and near-shore proxy data: Quaternary Science Reviews, v. 27, p. 2316-2340.

Granger, D.E., Kirchner, J.W., and Finkel, R.C., 1996, Spatially averaged long-term erosion rates measured from in situ-produced cosmogenic nuclides in alluvial sediment: J. Geol. v.104, p. 249–257.

Khomo, L. Bern, C.R., Hartshorn, A.S., Rogers, K.H., and Chadwick, O.A., 2013, Chemical tranfers along slowly eroding catenas developed on granitic crations in southern Africa: Geoderma, v. 202-203, p. 192-202.

Khomo, L. Hartshorn, A.S., Rogers, K.H., and Chadwick, O.A., 2011, Impact of rainfall and topography on the distribution of clays and major cations in granitic catenas in southern Africa: Catena v.87 p. 119-128.

Kohl, C.P., & Nishiizumi, K., 1992, Chemical isolation of quartz for measurement of *in-situ* produced cosmogenic nuclides: Geochim. Cosmochim. Acta v.56, p. 3583–3587.

Levick, S. R., Asner, G. P., Chadwick, O. A., Khomo, L. M., Rogers, K. H., Hartshorn, A. S., and Knapp, D. E., 2010, Regional insight into savanna hydrogeomorphology from termite mounds: Nature Communications, v.1(65), p. 1-7.

Partridge, T. C., Kerr, S. J., Metcalfe, S. E., Scott, L., Talma, A. S., & Vogel, J. C., 1993, The Pretoria saltpan: a 200,000 year southern African lacustrine sequence: Palaeogeography, palaeoclimatology, palaeoecology, v.101, p. 317-337.

Riebe, C.S., & Granger, D.E., 2013, Quantifying effects of deep and near-surface chemical erosion cosmogenic nuclides in soils, saprolite, and sediment: Earth Surface Processes and Landforms, v.38, p. 523-533.

Strahler, A.N., 1957, Quantitative analysis of watershed geomorphology: American Geophysical Union Transactions v.38, p. 913–920.

von Blanckenburg, F., 2005, The control mechanisms of erosion and weathering at basin scale from cosmogenic nuclides in river sediment: Earth Planet. Sci. Lett. v.237, p. 462–479.